# Comparative Study of Optimization Algorithms on the Design of Broadband Antennas

Maria Kovaleva, *Member, IEEE*, David Bulger, and Karu P. Esselle, *Fellow, IEEE*

***Abstract*—Broadband antennas find many applications in modern communication systems, such as Wi-Fi, 5G, and SatCom. Multiple competing optimization methods are available for the application to antenna design, while it would be preferable to know in advance if any method is superior. Here, an application of the cross-entropy method, along with particle swarm optimization and covariance matrix adaptation evolutionary strategy, to the design of broadband antennas is presented. The first example is an aperture-coupled microstrip patch antenna that has 9.5 dBi peak directivity and 53% bandwidth after optimization. It is then used as a feed in a high-gain broadband resonant cavity antenna. Using an all-dielectric superstrate with a transverse permittivity gradient, a compact thin resonant cavity antenna with a peak directivity of 19 dBi and 40% 3-dB bandwidth was designed. A comparative analysis of the cross-entropy method, particle swarm optimization, and covariance matrix adaptation evolutionary strategy applied to these two problems was carried out to provide the basis for further optimization of antennas in radio frequency and microwave frequency bands. We found that although all three methods reached a similar solution, the cross-entropy method has a speed advantage. It improves our ability to optimize existing designs and has wider applicability beyond antenna engineering.**

***Index Terms*—Covariance matrix adaptation, cross-entropy, electromagnetic, evolutionary, feed, microwave, optimization, particle swarm optimization, resonant cavity antenna, wideband.**

## I. Introduction

With the constantly increasing demand for high data rates in wireless communication systems, it is essential for antennas to operate at wide bandwidths. At the same time, relentless miniaturization requirements force antennas to have compact configurations. Although there are several alternative compact wideband printed antenna solutions employing monopoles or slots, microstrip patch antennas (MPAs) offer the advantages of flat profiles, low weight, medium gains of 5–10 dB, and low cost. According to [1], all broadband printed antennas can be classified as unidirectional and bidirectional. When the antenna radiates on one side of the ground plane, it is unidirectional, and when it radiates on both sides of the ground plane, it is bidirectional. The MPA, which has a hemispherical radiation pattern, is the basic antenna type of the first group. In its simplest form, an MPA consists of a radiating patch on one side of a dielectric substrate and a ground plane on the other side [2]. Since their introduction in 1953 [3], MPAs have undergone enormous development and have been used in applications such as terrestrial and satellite communications, telemetry, navigation, off-body communications, biomedical, and many others [4]–[8].

Increasing the bandwidth of MPAs has been the major challenge for antenna engineers for a long time, and broadband solutions with bandwidths of up to 60% have been achieved [9], [10]. One bandwidth-broadening technique is to introduce additional resonant elements, such as slots or parasitic patches, with adjacent resonant frequencies, and stack-tune the resonances. An MPA with an indirect excitation of the radiating patch through an aperture coupling and one or more parasitic patches placed above is known as an aperture-coupled MPA (ACMPA). It has been shown that ACMPAs can have very wide common impedance and gain bandwidths of more than 70% [11]–[14] but at a cost of low front-to-back ratio.

Any bandwidth-broadening technique introduces additional degrees of freedom to the designs and thus increases their complexity. The strong mutual coupling between closely spaced elements makes it difficult to predict the influence of design parameters on the input impedance using manual design methods. Optimization algorithms can not only find a near-optimal solution, but also speed up the design process. Particle swarm optimization (PSO), cross-entropy (CE), and covariance matrix adaptation evolutionary strategy (CMA-ES) have been previously applied to the design of broadband and ultra-wideband antennas, including E-patch [15] and planar monopole [16], and some performance comparisons are available in the literature [17]–[24]. Comparative studies do not intend to find the one best algorithm for all antenna optimization problems, but rather to shed some light on which algorithm steadily produces a better solution in shorter time frames for a particular problem class. This knowledge is useful for future optimization of antenna problems that have design similarities.

In this article, we implement CE, PSO, and CMA-ES to achieve antennas with low profile and wide impedance bandwidth in Ku band. Particularly, the optimization of a stand-alone

Manuscript received February 3, 2020; revised April 25, 2020; accepted May 25, 2020. Date of publication June 8, 2020; date of current version June 22, 2020. This work was supported in part by an Australian Government Research Training Program Scholarship and in part by the Australian Research Council. *(Corresponding author: Maria Kovaleva.)*

Maria Kovaleva was with the Centre for Collaboration in Electromagnetic and Antenna Engineering, Macquarie University, Sydney, NSW 2109, Australia, she is now with Curtin Institute of Radio Astronomy, Curtin University, Perth, WA 6102, Australia and with the University of Technology, Sydney, NSW 2007, Australia (e-mail: maria.kovaleva@curtin.edu.au).

David Bulger is with the Department of Mathematics and Statistics Faculty of Science and Engineering, Macquarie University, Sydney, NSW 2109, Australia (e-mail: david.bulger@mq.edu.au).

Karu P. Esselle is with the Electromagnetic and Antenna Engineering Department, University of Technology, Sydney, NSW 2007, Australia (e-mail: karu.esselle@mq.edu.au).

Digital Object Identifier 10.1109/JMMCT.2020.3000563

ACMPA and a resonant cavity antenna (RCA) with an ACMPA as a feed is presented. First, the ACMPA without a superstrate is optimized, and the obtained results and the performance of the algorithms are compared. Then, the ACMPA is combined with a partially reflective surface (PRS) to create a compact wideband RCA, which is optimized using the three aforementioned methods. The CE method, first presented in [25] for optimization of an RCA as a method to solve mixed-variable constraint problems, is here demonstrated for the optimization of continuous problems. Being a viable optimization method for electromagnetic problems, it is compared to two promising counterparts, PSO and CMA-ES. Although PSO, CMA-ES, and CE have been applied to other design problems, they have not been applied to ACMPA problems, especially in the context of comparing them for broadband optimization problems. The purpose of this article is to share our experience of comparing these algorithms for two optimization problems that arose in practice for us. We do not intend to select the best algorithm as a result of this study, as it is pointless on such a small sample size. We believe that more practical antenna design problems have to be optimized, and the results shared to the community to build a database for further statistical analysis. This article can also be used as a guide in optimizing other broadband antenna problems.

This article is organized as follows. Section II presents the design considerations of the antenna in focus, as well as the optimization methodology. Section III presents the transformation of a middle-gain antenna to a high-gain antenna and its optimization results. Section IV discusses the considered optimization algorithms. Section V concludes the article.

## II. Optimization of an ACMPA

This section presents the results of optimization of an ACMPA using CE, PSO, and CMA-ES. After formulating the optimization problem, we describe the application of the CE method to a continuous bounded search space, and then compare the optimization results of an ACMPA obtained by CE, PSO, and CMA-ES. As CE is a relatively new optimization method for EM applications, this comparison is required for the assessment of its convergence properties. The comparison will be based on the number of function evaluations required for the convergence to the global solution and on the best fitness value obtained by each algorithm.

### A. Problem Formulation

The geometry of the ACMPA with design variables is shown in Fig. 1. The lower and upper limits for each design variable are given in the inset table. The substrates of diameter $D = 60$ mm are made of Rogers RT5880 laminate with a thickness of $h = 0.787$ mm and a relative permittivity of $\varepsilon_r = 2.2$. The fixed parameters of the antenna are summarized in Table I. The first substrate has a printed 50-$\Omega$ microstrip line ($w = 2.45$ mm) on one side and a ground plane with a coupling aperture of width $S_y = 0.5$ mm and length $S_x$ on the opposite side. The aperture is centred along the *x*-coordinate under the patch to obtain low cross-polarization levels. The excitation of the aperture is controlled by the length of an open-circuit stub $L_s$. The dimensions of the aperture have a significant effect on the coupling to the first patch of width $W_1$ and length $L_1$. The size of the first patch is a very important factor in impedance matching as it comes in between the aperture and the top patch of dimensions $W_2 \times L_2$.

| Design variables | Limits, *mm* |
|---|---|
| $h_1$ | [0, 1] |
| $h_2$ | [0, 1] |
| $L_1$ | [5, 7] |
| $L_2$ | [5, 7] |
| $shift_1$ | [-1.5, 1.5] |
| $shift_2$ | [-1.5, 1.5] |
| $Ls$ | [1, 3] |
| $Sx$ | [6, 9] |
| $W_1$ | [9, 13] |
| $W_2$ | [9, 13] |

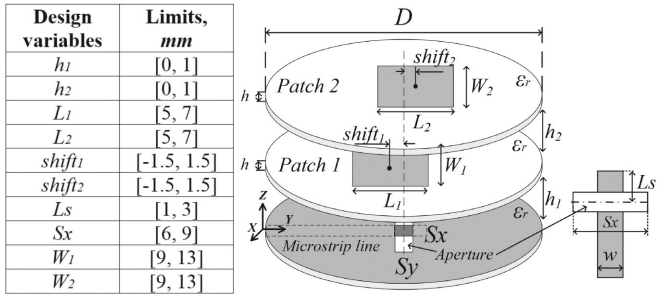


Fig. 1. Geometry of the optimized ACMPA. Inset table shows the lower and upper limits of the design variables.

TABLE I
Fixed ACMPA Parameters

| $D$, mm | $h$, mm | $\varepsilon_r$ | $w$, mm | $S_y$, mm |
|---|---|---|---|---|
| 60 | 0.787 | 2.2 | 2.45 | 0.5 |

Broadband impedance matching in the ACMPA is achieved by stagger-tuning of three resonances. The aperture in the ground plane is of resonant length that allows coupling of the resonant patches to the feedline, resulting in closely spaced resonances. For maximum bandwidth and efficiency, the patches are separated from each other by air gaps $h_1$ and $h_2$, and the thin dielectric substrates are only used for the support of the printed patches. Lower values of $h_1$ and $h_2$ are preferred in order to have a low-profile antenna, but they also increase the coupling between the aperture and the patches, and thereby lower the impedance bandwidth. Thus, two contradicting requirements are imposed on the design, i.e., wide impedance bandwidth and low antenna profile. To solve this problem, two more variables, $shift_1$ and $shift_2$, have been introduced as proposed in [26]. They determine the shift of the patches in the *y* direction from the middle of the superstrates and help to achieve a larger impedance bandwidth with reduced thickness of the antenna.

In order to choose the lower and upper limits, theoretical calculations and a quick sensitivity analysis using a grid search have been performed. The theoretical dimensions of the patches have been calculated using the design procedure in [27] that consists of four consecutive steps. First, the width of the patch is found using

$$W = \frac{c}{2f_i}\sqrt{\frac{2}{\varepsilon_r + 1}} \tag{1}$$

where $c$ is the speed of light, $\varepsilon_r = 2.2$, and $f_i$ is the frequency range from 11 to 19 GHz with 0.5-GHz step. Next, the effective dielectric constant is found by

$$\varepsilon_{r\text{eff}} = \frac{\varepsilon_r + 1}{2} + \frac{\varepsilon_r - 1}{2}\left[1 + 12\frac{h}{W}\right]^{-\frac{1}{2}} \tag{2}$$

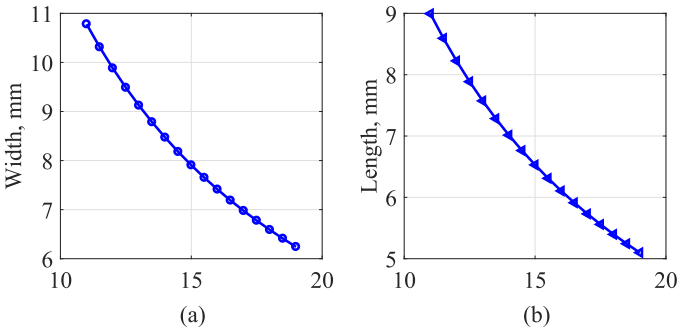


Fig. 2. Theoretical dimensions of a microstrip patch calculated using the design procedure in [27].

where $h$ is the substrate thickness. The extended incremental length of the patch that accounts for the fringing effects is found by

$$\triangle L = 0.412h\frac{(\varepsilon_{reff}+0.3)(\frac{W}{h}+0.264)}{(\varepsilon_{reff}-0.258)(\frac{W}{h}+0.8)}. \quad (3)$$

Finally, the actual length of the patch is found by

$$L = \frac{1}{2f_i\sqrt{\varepsilon_{reff}}\sqrt{\mu_0\varepsilon_0}} - 2\triangle L. \quad (4)$$

Calculated width and length of a microstrip patch on a given substrate as a function of design frequency are shown in Fig. 2. For the frequency span from 11 to 19 GHz, the optimal width of a patch changes from 11 to 6 mm, and the length changes from 9 to 5 mm. These dimensions have been calculated using a cavity model, which is a simplification of a patch antenna, and thus, can be used as a starting point for optimization.

Sensitivity analysis has been performed to find appropriate ranges for the design variables. To meet the requirement of a low profile, the air gaps $h_1$ and $h_2$ between the substrates have been limited to the range of [0,1] mm. It can be seen from Fig. 3(a) that even small variations significantly affect the input impedance. The sensitivity of other design variables is displayed in Fig. 3, where the gray dashed lines determine the desired input reflection coefficient $|S_{11}|$ response. The widths of patches are less sensitive parameters and, therefore, their ranges have been extended to [9, 13] mm. According to [3], the two patches are usually very close in size, with the top element being slightly larger than the bottom element. Also, it has been previously observed that for impedance matching, the relative dimensions of two patches are important as opposed to their absolute dimensions [2]. Parameters $shift_1$ and $shift_2$ vary between narrow limits $[-1.5, 1.5]$ mm to avoid significant asymmetry in the radiation patterns.

The optimization goal is to obtain a magnitude of the reflection coefficient $S_{11}$ below $-10$ dB across the frequency band 12–18 GHz. To ensure this, the input impedance is analyzed in the range 11–19 GHz, and the fitness function to be maximized has been defined as

$$F.F. = -\left(\sum_{f_i=11\text{ GHz}}^{19\text{ GHz}} L(f_i)\right) \quad (5)$$

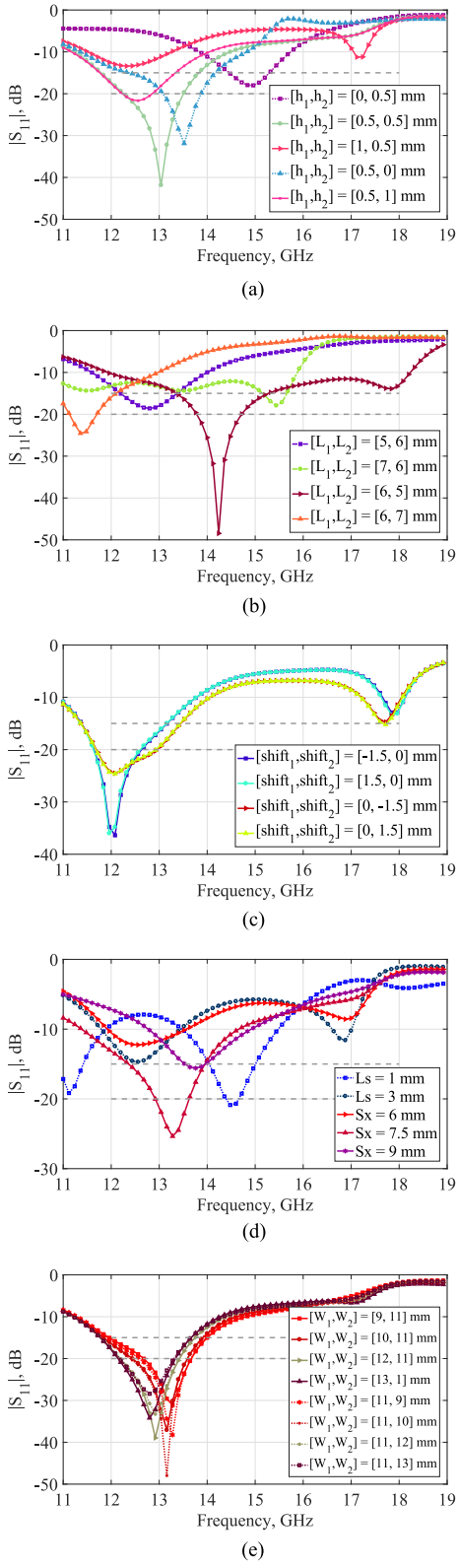


Fig. 3. Sensitivity analysis of the design variables. Gray dashed lines show the desired $S_{11}$ response. (a) $L_1 = L_2 = 6$ mm; $shift_1 = shift_2 = 0$ mm; $L_s = 2$ mm; $S_x = 7$ mm; $W_1 = W_2 = 11$ mm. (b) $h_1 = h_2 = 0.5$ mm; $shift_1 = shift_2 = 0$ mm; $L_s = 2$ mm; $S_x = 7$ mm; $W_1 = W_2 = 11$ mm. (c) $h_1 = h_2 = 0.5$ mm; $L_1 = L_2 = 6$ mm; $L_s = 2$ mm; $S_x = 7$ mm; $W_1 = W_2 = 11$ mm (d) $h_1 = h_2 = 0.5$ mm; $L_1 = L_2 = 6$ mm; $shift_1 = shift_2 = 0$ mm; $W_1 = W_2 = 11$ mm. (e) $h_1 = h_2 = 0.5$ mm; $L_1 = L_2 = 6$ mm; $shift_1 = shift_2 = 0$ mm; $L_s = 2$ mm; $S_x = 7$ mm.

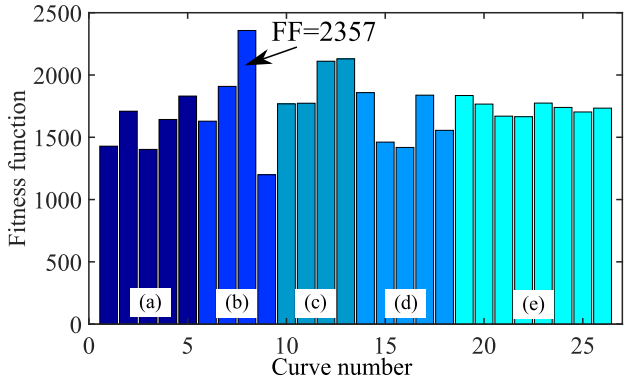


Fig. 4. Fitness function value for each design shown in Fig. 3.

where

$$L(f_i) = \begin{cases} S_{11}(f_i), & \text{if } S_{11}(f_i) \geq -15\,\text{dB} \\ -20, & \text{if } -20\,\text{dB} \leq S_{11}(f_i) < -15\,\text{dB} \\ -35 - S_{11}(f_i), & \text{if } -35\,\text{dB} \leq S_{11}(f_i) < -20\,\text{dB} \\ 0, & \text{if } S_{11}(f_i) < -35\,\text{dB} \end{cases} \tag{6}$$

and $f_i$ = 11,...,19 GHz with $i$ = 1,...,201 frequency points. Equation (6) gradually penalizes designs with the reflection coefficient lower than –20 dB in order to achieve larger impedance bandwidth [28]. This fitness function works well for wideband antennas because the desired $S_{11}$ is usually between –15 and –20 dB, and it is known in advance that it is not realistic to obtain a –30 dB matching level in a wide frequency band. Fig. 4 shows the calculated fitness function values for all designs from the sensitivity analysis. The best result found using a coarse grid search has fitness function $F.F. = 2357$.

### B. Optimization Methodology

The given ACMPA optimization problem is a classic continuous optimization problem with a bounded solution space. It has ten continuous design variables ($d = 10$)

$$\mathbf{x} = (h_1,\ h_2,\ L_1,\ L_2,\ shift_1,\ shift_2,\ L_s,\ S_x,\ W_1,\ W_2). \tag{7}$$

The optimization has been carried out independently by CE, PSO, and CMA-ES with the fitness function given in (5).

Below, we describe the details of the optimization procedure, focusing on CE implementation because it is a relatively new optimization method for electromagnetic community, and less information about it is available in the literature. We gave a short review on applications of CE optimization algorithm to antenna designs in [25], where we described an application of CE to mixed-variable problems. Previous applications of CE to continuous problems use Gaussian distribution to sample populations [29]–[31]. In this article, we demonstrated the advantage of using beta distribution in CE. Although a normal (Gaussian) distribution can also be used for sampling continuous variables, the use of a beta distribution ensures that every sample stays within the defined limits. Due to its bounded support ([0,1]), the optimal design never exceeds the limits of design variables.

TABLE II
INPUT PARAMETERS FOR CE, PSO, AND CMA-ES IN ACMPA OPTIMIZATION

| | |
|---|---|
| **CE** | |
| Population size, $N_{pop}$ | 50 |
| Elite subpopulation size, $N_{el}$ | 10 |
| Smoothing coefficient, $\alpha_S$ | 0.5 |
| **PSO** | |
| Population size, $N_{pop}$ | 50 |
| Acceleration coefficients, $(c_1, c_2)$ | (1.49, 1.49) |
| Inertia weight, $(w_{max} - w_{min})$ | (0.9 – 0.1) |
| Number of iterations, $N_{it}$ | 30 |
| Velocity clamping factor, $V_{cf}$ | 1.8 |
| **CMA-ES** | |
| Population size, $N_{pop}$ | 11 |

A beta distribution family has the following probability distribution function (PDF):

$$B(\mathbf{x}; v^t) = \frac{x^{\alpha-1}(1-x)^{\beta-1}}{\int_0^1 x^{\alpha-1}(1-x)^{\beta-1}\,\mathrm{d}x}. \tag{8}$$

Using linear transformation, we can set any boundaries of the design variables.

The flow of the CE method is as follows.

1) Initialise iteration count $t = 0$. Initial distribution parameters $v^t = (\alpha^t, \beta^t) = (1, 1)$.
2) Randomly sample $N_{\text{pop}}$ candidates from the beta distribution $B(\mathbf{x}; v^t)$.
3) Evaluate the fitness function $F.F.$ of each candidate.
4) Sort the candidates and choose the elite of size $N_{el}$.
5) Using maximum likelihood estimation, find such $(\alpha^{t+1}, \beta^{t+1})$ that best describe the elite distribution.
6) (optional) Smooth $(\alpha^{t+1}, \beta^{t+1})$ according to the equations

$$\alpha^{t+1} = \alpha^t + \alpha_s * (\alpha^{t+1} - \alpha^t) \tag{9}$$

$$\beta^{t+1} = \beta^t + \alpha_s * (\beta^{t+1} - \beta^t). \tag{10}$$

7) Update iteration count $t = t + 1$.
8) Repeat steps 2–7 until the stopping criterion is met.

The input parameters required for CE, PSO, and CMA-ES that were set in this optimization are given in Table II. For CE, the recommended $N_{el}$ is 10–20% of population size, and recommended value for $\alpha_S$ is between 0.4 and 0.7. Higher smoothing accelerates the search, while lower smoothing slows down the search. The effect of elite subpopulation size is the opposite: smaller $N_{el}$ speeds up the search, while bigger $N_{el}$ decelerates the search. For PSO, $N_{\text{pop}}$ is generally four times the dimensionality of the problem, and the maximum number of iterations should be selected in balance with it. If $N_{\text{pop}}$ is too large/low, there is a danger of not reaching the convergence within $N_{it}$. A good starting point for hyperparameters can be obtained by optimizing a test function of the same dimensionality as the optimization problem. The population size $N_{\text{pop}}$ for CMA-ES is recommended [23] to be at least

$$N_{\text{pop}} = (4 + round(3 * \log(d))) = 11 \tag{11}$$

given that the number of design variables $d = 10$ in this case. Other parameters were set to their default values. To find the hyperparameters for the implementations described in the next sections, we first optimized a 10-dimensional Ackley test problem with default hyperparameters. Then, looking at the convergence curves, we adjusted the hyperparameters to achieve smaller number of function evaluations and 100% success rate for the Ackley problem. These hyperparameters were then used for optimizing real problems.

It is worth mentioning that CE and CMA-ES have some resemblance in operating principles. Both algorithms use probability distributions for sampling the populations, rank the solutions, choose elite subpopulations, and fit subsequent sampling distributions to match the elite distribution. The key difference is that CMA-ES uses multivariate normal sampling distributions, with each generation's distribuiton matched to the mean and covariance of the previous generation's elite group, whereas CE can use any convenient distribution family, with sampling parameters inferred from the previous generation's elite group by maximum likelihood estimation.

In our implementation, the stopping criterion for the CE optimization is the population diversity. The run is considered converged when the average difference between the candidates in an elite subpopulation is less than the threshold $\delta = 0.5$ mm. This stopping criterion helps to avoid unnecessary computations of very similar designs and, thus, to reduce the total optimization time. For PSO and CMA-ES, the stopping criterion was a maximum number of iterations $N_{it}$ equal to 30 and 1000, respectively. The CE algorithm converged after 1200 function evaluations, with PSO after 1500 and CMA-ES after 1815.

To evaluate the antenna characteristics, CST Microwave Studio time domain solver was used. Since the considered optimization problems are broadband, time domain solver is preferable over the frequency domain one. Using an Intel Core i7, 3.6 GHz processor with 32 GB of RAM, time required to complete an optimization was approximately 32 h for CE, 40 h for PSO, and 48.4 h for CMA-ES.

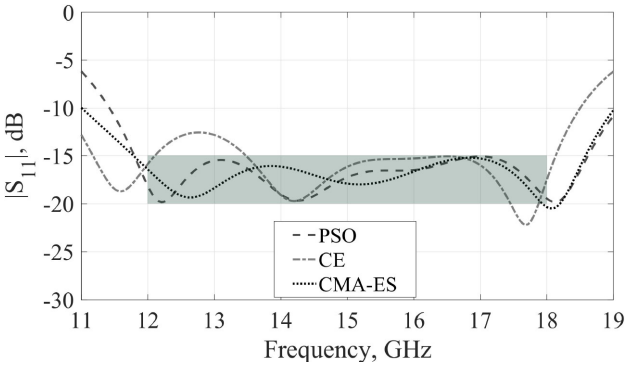


Fig. 5. Reflection coefficient of the ACMPAs optimized by PSO, CE, and CMA-ES. Shaded area shows the region that generates the highest F.F.

TABLE III
DIMENSIONS AND F.F. OF THE BEST ACMPA SOLUTIONS

| Design variables, mm | CE | PSO | CMA-ES |
|---|---|---|---|
| $h_1, h_2$ | 0.47, 0.75 | 0.55, 0.98 | 1.4, 1.9 |
| $L_1, L_2$ | 6.2, 5.3 | 5.94, 5.0 | 6.9, 4.7 |
| $shift_1, shift_2$ | –0.4, 1.3 | –0.46, 1.5 | –0.92, 3.4 |
| $L_s$ , $S_x$ | 1.6, 6.8 | 1.4, 6.3 | 3.6, 15.9 |
| $W_1, W_2$ | 9.5, 10.9 | 9.4, 10.8 | 12.3, 9.8 |
| *F.F.*, Eq. (5) | 3470.2 | 3743.2 | **3780.9** |

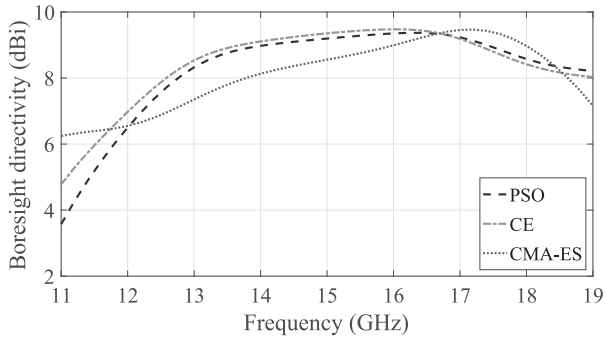


Fig. 6. Boresight directivity of the optimized ACMPAs.

### C. Optimization Results

The input reflection coefficients of the optimized ACMPAs are shown in Fig. 5. It can be seen that all the optimized antennas are well matched in the range of 12–18 GHz with $|S_{11}| \leqslant -10$ dB. The best design was achieved by CMA-ES and has a fractional bandwidth of 53%.

Optimized design parameters of the best ACMPAs obtained by PSO, CE, and CMA-ES are given in Table III. All optimized designs have a significantly higher fitness function value compared to the one obtained manually with $F.F. = 2357$. Most of the design variables in the solutions obtained by PSO and CE have very similar values. Although CMA-ES produced the result with the highest $F.F.$, some design parameters exceed the given boundaries. Relative to the wavelength of the center frequency of the operating band ($\lambda_{15\text{GHz}} = 20$ mm), a significantly different parameter is the length of the aperture that couples the microstrip line and the first patch ($S_x$).

Exceeding the boundaries of the initial seed is attributed to use of the Gaussian distribution for sampling in CMA-ES, that intrinsically has an unbounded support. We purposefully did not impose any constraints in CMA-ES to observe whether the algorithm deviates from the initial seed that was randomly generated within the design boundaries. For continuous unconstrained optimization problems, it is not fatal and can be an advantage: if the initial seed is badly selected, the algorithm will correct it. Gaussian distribution can be used in CE as well, but the implementation in this article focuses on beta PDF for continuous variables, which cannot be done in CMA-ES.

The boresight directivity of three optimized ACMPAs, shown in Fig. 6, changes from 7 to 9.5 dBi in the frequency range 12–18 GHz. Larger variations in the boresight directivity of the CMA-ES solution is attributed to the significant shift of the second patch from the middle of the structure. The radiation

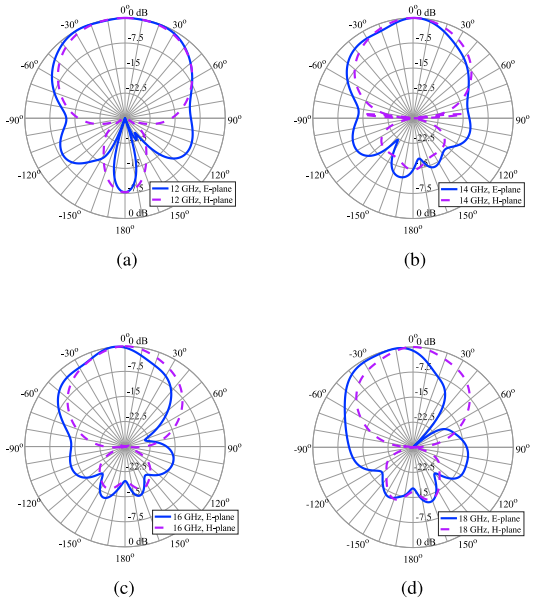


Fig. 7. Radiation patterns of the CE-optimized ACMPA. (a) 12 GHz; (b) 14 GHz; (c) 16 GHz; (d) 18 GHz.

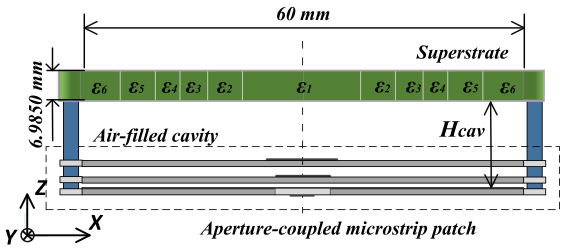


Fig. 8. Geometry of the RCA with an ACMPA feed. The PRS is an all-dielectric TPG superstrate of diameter $D = 60$ mm and thickness $t = 6.985$ mm.

patterns at 12, 14, 16, and 18 GHz for the CE solution are given in Fig. 7. The E-plane corresponds to the $zy$-plane in Fig. 1, and the H-plane corresponds to the $zx$-plane. In the majority of the frequency band, the patterns in the E-plane remain near-broadside. The cross-polarization levels are below $-25$ dB for most of the band and rise to $-12$ dB at 18 GHz. The simulated total efficiency of all optimized antennas is more than 95%.

## III. Optimization of RCA With ACMPA Feed

A wideband high-gain RCA can be designed by integrating the ACMPA described in the previous section with an all-dielectric transverse permittivity gradient (TPG) superstrate. In this section, we apply PSO, CE, and CMA-ES to optimize the input impedance of such an RCA with ACMPA feed and analyze the algorithms' performances.

### A. Design of an RCA With an ACMPA Feed

Fig. 8 shows an RCA constructed from an ACMPA with a six-sectional all-dielectric TPG PRS placed on top. The fixed design parameters of the ACMPA remain the same as given in Fig. 1 and Table I. The TPG superstrate has the parameters presented in [25] of the Case-II superstrate design. The methodology for

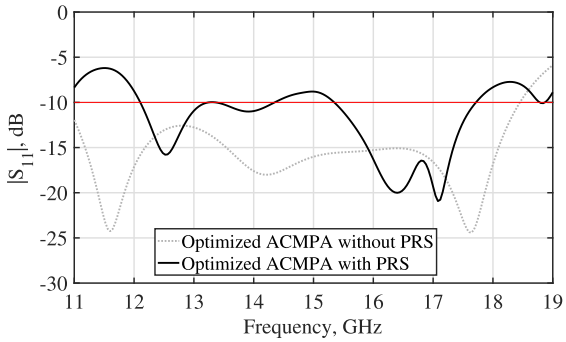


Fig. 9. Reflection coefficient of the CE-optimized ACMPA (Table III) before and after placing the PRS on top.

obtaining these parameters is also presented in that article. Out of three Case-II TPGs, we selected here the one with the highest directivity-bandwidth product. It has thickness $t = 6.985$ mm and permittivity distribution $(\varepsilon_1, \ldots, \varepsilon_6) = (10.2, 9.2, 6, 4.5, 3.5, 3.5)$. The permittivity gradient is created by dividing the superstrate into six circular sections of widths $(w_1, \ldots, w_6) = (7.92, 6.62, 4.47, 2.92, 3.39, 3.68)$ mm. The cavity height $H_{\text{cav}}$ equals 13 mm, which corresponds to $0.5\lambda_0$, where $\lambda_0 = 26$ mm is the free-space wavelength of the first resonance frequency of the cavity (11.5 GHz).

Fig. 9 shows that the input impedance of the CE-optimized ACMPA deteriorates when it is loaded with a highly reflective superstrate. Therefore, to achieve a broadband impedance bandwidth for this RCA, the ACMPA with the addition of the PRS needs to be optimized again. We will use PSO, CE, and CMA-ES and compare the performance of the algorithms.

### B. Optimization Details

When the superstrate is placed above the ACMPA, a resonant cavity is created. The strong reflections between the TPG superstrate and the ground plane make impedance matching very difficult. Defining the fitness function as in (6) results in narrowband solutions and low FF. Therefore, the requirements in the fitness function have been relaxed to the following:

$$F.F. = -\left(\sum_{f_i=11\text{ GHz}}^{19\text{ GHz}} L(f_i)\right) \tag{12}$$

where

$$L(f_i) = \begin{cases} S_{11}(f_i), & \text{if } S_{11}(f_i) \geq -10 \text{ dB} \\ -15, & \text{if } -15 \text{ dB} \leq S_{11}(f_i) < -10 \text{ dB} \\ -30 - S_{11}(f_i), & \text{if } -30 \text{ dB} \leq S_{11}(f_i) < -15 \text{ dB} \\ 0, & \text{if } S_{11}(f_i) < -30 \text{ dB} \end{cases} \tag{13}$$

and $f_i = 11, \ldots, 19$ GHz with $i = 1, \ldots, 201$ frequency points. Again, this formulation of the fitness function intentionally suppresses candidates with $S_{11} < -30$ dB at any frequency within the band for the sake of a wideband matching. The best solution will have $S_{11}$ bounded by $[-10, -15]$ dB.

TABLE IV
INPUT PARAMETERS FOR CE, PSO, AND CMA-ES IN RCA WITH ACMPA FEED OPTIMIZATION

| | |
|---|---|
| **CE** | |
| Population size, $N_{pop}$ | 50 |
| Elite subpopulation size, $N_{el}$ | 6 |
| Smoothing coefficient, $\alpha_S$ | 0.8 |
| **PSO** | |
| Population size, $N_{pop}$ | 30 |
| Acceleration coefficients, $(c_1, c_2)$ | (1.49, 1.49) |
| Inertia weight, $(w_{max} - w_{min})$ | (0.9 – 0.1) |
| Number of iterations, $N_{it}$ | 30 |
| Velocity clamping factor, $V_{cf}$ | 1.8 |
| **CMA-ES** | |
| Population size, $N_{pop}$ | 11 |

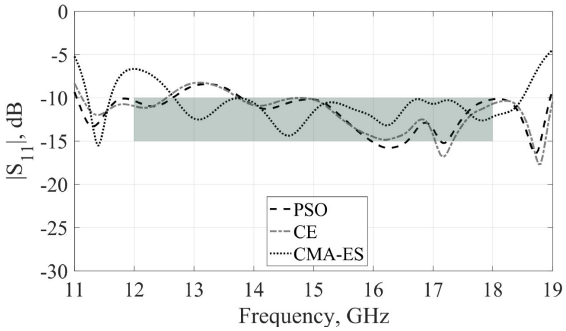


Fig. 10. Reflection coefficient of the RCAs optimized by PSO, CE, and CMA-ES. Shaded area shows the region that generates the highest F.F.

The settings for each algorithm are summarized in Table IV. The population size $N_{\rm pop}$ for CMA-ES is calculated using (11) with $d = 10$.

### C. Results

Fig. 10 provides the impedance matching results of the best optimized RCAs. The CE- and PSO-generated solutions have little variation in the patch length and coupling aperture and stub dimensions, which translates into a very similar $S_{11}$ curve. The reflection coefficient $S_{11} \leqslant -10$ dB in the band 11–19 GHz except for the increase to –8.5 dB around 13 GHz. This means that VSWR $\leqslant$ 2.2 for the entire frequency range, which is below a common requirement of VSWR $\leqslant$ 2.5 for broadband antennas. The CMA-ES solution has a reflection coefficient with a sharp resonance at 11.3 GHz and then increasing up to –6.8 dB (VSWR $\leqslant$ 3) between 11.6 and 12.7 GHz. Here, the freedom of exceeding the design boundaries resulted in the lowest F.F. for CMA-ES.

The requested impedance matching goal is extremely difficult to obtain for a RCA due to such a wide frequency range 12–18 GHz, and the results show that the stepped fitness function $L(F_i)$ works well for broadband optimization. The reason that $S_{11}$ increases at 12–13 GHz is the strong reflections in the cavity due to a highly reflective PRS. The fact that two algorithms (CE and PSO) independently converged to a very similar result states that it might be a near-optimal solution.

The dimensions of the best ACMPA designs obtained by PSO, CE, and CMA-ES are summarized in Table V. The highest fitness $F.F. = 2825.8$ is found by PSO, and the CE solution has $F.F. = 2789.7$. Both CE and PSO converged after 900 number of function evaluations (NFE). In comparison to an ACMPA, this antenna model is much more complex, and its single simulation is more time-consuming. Using CE, the optimization took 241 178 s, which is almost 3 days. PSO took approximately the same overall optimization time because of the same number of function evaluations. CMA-ES with $N_{\rm pop} = 11$ took more than twice as long and was stopped after 205 iterations because of no improvement for 45 consecutive iterations.

TABLE V
DIMENSIONS AND F.F. OF THE BEST ACMPA-FED RCA SOLUTIONS

| **Design variables (mm)** | **CE** | **PSO** | **CMA-ES** |
|---|---|---|---|
| $h_1, h_2$ | 0.19, 0.56 | 0.26, 0.24 | 0.58, 0 |
| $L_1, L_2$ | 5.75, 5.29 | 5.82, 5.03 | 2.75, 4.21 |
| $shift_1, shift_2$ | 0.41, –0.72 | –0.57, –1.5 | –2.05, 0.36 |
| $L_s, S_x$ | 2.0, 6.32 | 1.83, 6.52 | 1.16, 6.56 |
| $W_1, W_2$ | 9.06, 10.87 | 10.38, 12.99 | 12.36, 9.54 |
| *F.F.*, Eq. (12) | 2789.7 | **2825.8** | 2669.4 |

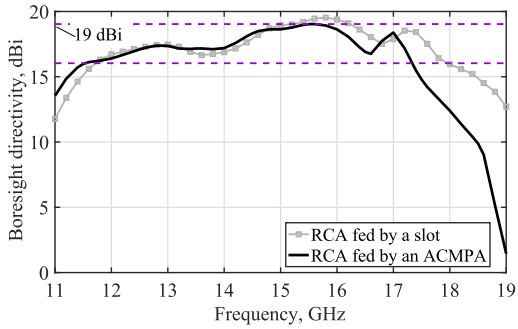


Fig. 11. Boresight directivity comparison of the slot-fed RCA and the ACMPA-fed RCA optimized by CE.

The boresight directivity of the CE solution is shown in Fig. 11. The peak directivity is 19 dBi, and the 3-dB bandwidth is from 11.5 to 17.2 GHz, which is 40%. For comparison, the boresight directivity of a slot-fed RCA is also given in the graph. Its peak directivity is 19.4 dBi, and the bandwidth is also 40%. With just a 0.4-dB reduction in the peak directivity, ACMPA design provides an alternative feed solution, resulting in a much lower RCA profile. A slot in the ground is usually fed by a coaxial-to-waveguide adapter, which would add 25–30 mm to the total antenna profile. We used a Pasternack WR-62 adapter to excite the slot with dimensions 12-by-7.5 mm in the simulation. The profile reduction of more than 50% is clear from Fig. 12.

Radiation patterns at 12, 14, and 16 GHz of the CE-optimized design are provided in Fig. 13. It can be seen that the RCA has a directive beam with low side lobe levels and a front-to-back ratio less than –15 dB.

## IV. DISCUSSION

In this section, we first discuss the structural differences in obtained design parameters and then compare the performance of CE, PSO, and CMA-ES. In ACMPA-optimized solutions (Table III), we notice that the most significantly different structural parameter is the length of the coupling aperture $S_x$ produced by CMA-ES. We defined the boundaries for $S_x$ so that

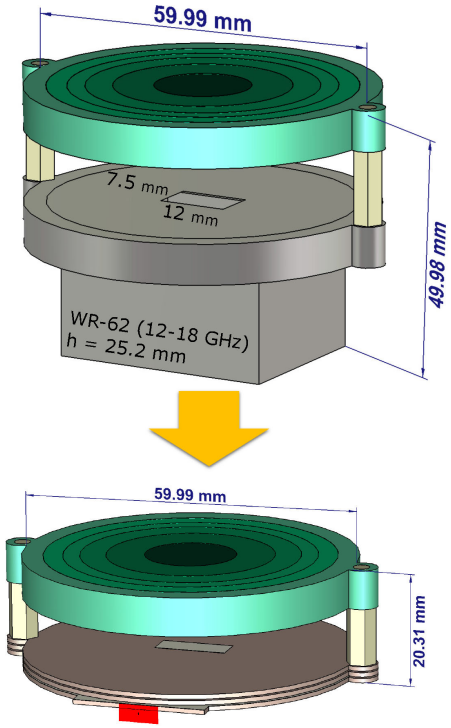


Fig. 12. Comparison of the slot-fed RCA and the ACMPA-fed RCA.

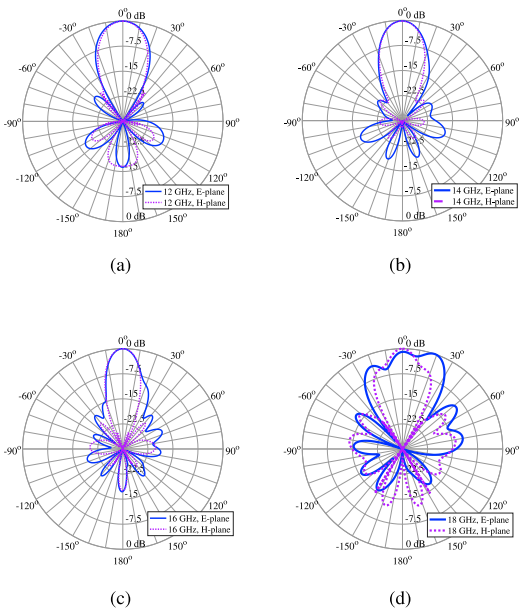


Fig. 13. Radiation patterns of the CE-optimized RCA with ACMPA. (a) 12 GHz; (b) 14 GHz; (c) 16 GHz; (d) 18 GHz.

the aperture resonance appears at the high end of the frequency range. However, CMA-ES violated the design boundaries and converged to $S_x = 15.9$ mm, which is half-wavelength at 9.4 GHz. Since wideband matching is achieved by stacking three resonances, and there is no specific order for the appearance of resonances, it is also a viable solution. As we could see, larger aperture required longer coupling stub $L_s$ in CMA-ES solution. Other noticeably different design parameters are $shift_2$ and $W_1$, and sensitivity analysis in Fig. 3(c) and (e) shows that they are not very sensitive parameters as compared to others and thus, can vary more.

TABLE VI
BEST OBTAINED F.F. AND NFE OF EACH ALGORITHM APPLIED TO THE OPTIMIZATION OF ACMPA AND RCA WITH ACMPA FEED

| | Best F.F. | NFE |
|---|---|---|
| **ACMPA** | | |
| CE | 3470.2 | **1200** |
| PSO | 3743.2 | 1500 |
| CMA-ES | **3780.9** | 1815 |
| **RCA with ACMPA feed** | | |
| CE | 2789.7 | **900** |
| PSO | **2825.8** | **900** |
| CMA-ES | 2669.4 | 2255 |

Similar difference in structural parameters can be observed for the RCAs with ACMPA feed (Table V). CE and PSO produced very similar solutions. The differences occur in the patch dimensions $[L_{(1,2)}, W_{(1,2)}]$ and $[shift_1, shift_2]$. Again, as three resonances can occur in any order, these parameters can vary freely within the boundaries. From these examples, we conclude that broadband optimization problems with near 40% bandwidths are highly multimodal.

The comparison of the acquired F.F. and NFE is given in Table VI. In both optimized examples, PSO found the best F.F., but if we look closely at the impedance matching curves and design parameters, we will notice that CE and PSO solutions are very similar. Another consideration is NFE, which is important for simulation-driven optimization with extended computational load. Applied to the ACMPA optimization problems with continuous variables, the CE method converged faster than PSO and CMA-ES.

In the first example, PSO required 1500 NFE, while CE only needed 1200, and in the second example, both PSO and CE converged after 900 NFE. Although CMA-ES had the smallest population size, it required more function evaluations, and, therefore, a longer optimization time. NFE was 1815 in the first case and 2255 in the second case. Also, even though CMA-ES generated the best ACMPA design in the first example, it violated the search space limits. The reason is that the Gaussian distribution has an unbounded support, and, therefore, some random samples might appear on the tails of the distribution and exceed the boundary limits. This can be solved by disregarding or penalizing designs that are located outside of the search space limits.

The evolution of F.F. for the optimization of the ACMPA and the RCA with ACMPA are given in Fig. 14(a) and (b), respectively. Good convergence can be observed for the CE and PSO methods. The convergence of CMA-ES has not been recorded. The effect of smoothing parameters $\alpha_S$ on the number of iterations in the CE method can be seen. In ACMPA optimization, $\alpha_S = 0.5$ and $N_{it} = 24$, while in the RCA with ACMPA feed optimization, smoothing was increased to $\alpha_S = 0.8$, which resulted in $N_{it} = 18$.

The limitation of this optimization study is the small number of trials obtained for each algorithm. To obtain a statistically viable performance measure for the comparison study, multiple optimization trials have to be executed—the method called

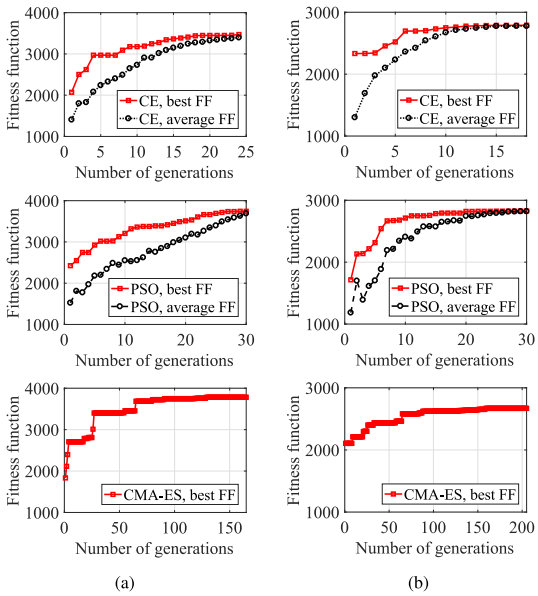


Fig. 14. CE, PSO, and CMA-ES convergence curves for two design cases. (a) ACMPA; (b) RCA with ACMPA feed.

multistart. This is a common procedure for test functions, but in application to real engineering problems, which are simulation-driven, performing multiple repetitive trials is impractical due to a fixed computational budget.

## V. Conclusion

This article presented a comparative study of CE, CMA-ES, and PSO optimization algorithms in application to broadband antenna design. An ACMPA problem with 10 variables was first considered and the three methods were used for its optimization. The best designed ACMPA has a peak directivity of 9.5 dBi and a 53% impedance bandwidth. Then, the ACMPA was integrated into an RCA with an all-dielectric TPG superstrate. The best optimized ACMPA-fed RCA had a peak directivity of 19 dBi and a 3-dB radiation bandwidth of 40%, well covered by an impedance bandwidth. Compared to the alternative feeds presented in the literature, such as a slot in a ground plane fed by a waveguide or MPAs, the proposed ACMPA feed gives an advantage of a reduced antenna profile.

For an RCA with only a single feed (as opposed to an array of feeds), the proposed design presents competitive performance: its highly directive beam of 19 dBi is stable over 11.5–17.2 GHz frequency range, featuring a compact footprint and light weight. This antenna would be suitable for Wi-Fi, 5G, and SatCom applications. It is worth highlighting that to manually find this solution with ten degrees of freedom of continuous type would be a problem of unrealistically high complexity due to "the curse of dimensionality." Comparing the performance of CE, CMA-ES, and PSO in application to the aforementioned two antenna designs, we found that although all three algorithms produced similar best solutions, CE required the least number of function evaluations. This confirms its fast convergence properties and suitability for multimodal EM optimization problems. This is especially useful for computationally heavy EM problems, such as metasurfaces and large-aperture antennas.

## References


[1] A. Katyal and A. Basu, "Compact and broadband stacked microstrip patch antenna for target scanning applications," *IEEE Antennas Wireless Propag. Lett.*, vol. 16, pp. 381–384, 2017.

[2] G. Kumar and K. Ray, *Broadband Microstrip Antennas*. Norwood, MA, USA: Artech House, 2003.

[3] D. M. Pozar and D. H. Schaubert, *Microstrip Antennas: The Analysis and Design of Microstrip Antennas and Arrays*. Hoboken, NJ, USA: Wiley, 1995.

[4] B. Biglarbegian, M. Fakharzadeh, D. Busuioc, M. R. Nezhad-Ahmadi, and S. Safavi-Naeini, "Optimized microstrip antenna arrays for emerging millimeter-wave wireless applications," *IEEE Trans. Antennas Propag.*, vol. 59, no. 5, pp. 1742–1747, May 2011.

[5] N. R. Labadie, S. K. Sharma, and G. M. Rebeiz, "A circularly polarized multiple radiating mode microstrip antenna for satellite receive applications," *IEEE Trans. Antennas Propag.*, vol. 62, no. 7, pp. 3490–3500, Jul. 2014.

[6] M. Li and K. M. Luk, "Low-cost wideband microstrip antenna array for 60-GHz applications," *IEEE Trans. Antennas Propag.*, vol. 62, no. 6, pp. 3012–3018, Jun. 2014.

[7] S. J. Chen, T. Kaufmann, D. C. Ranasinghe, and C. Fumeaux, "A modular textile antenna design using snap-on buttons for wearable applications," *IEEE Trans. Antennas Propag.*, vol. 64, no. 3, pp. 894–903, Mar. 2016.

[8] J. Zhang, S. Yan, and G. A. E. Vandenbosch, "A miniature feeding network for aperture-coupled wearable antennas," *IEEE Trans. Antennas Propag.*, vol. 65, no. 5, pp. 2650–2654, May 2017.

[9] M. A. Matin, B. S. Sharif, and C. C. Tsimenidis, "Probe fed stacked patch antenna for wideband applications," *IEEE Trans. Antennas Propag.*, vol. 55, no. 8, pp. 2385–2388, Aug. 2007.

[10] V. P. Sarin, N. Nassar, V. Deepu, C. K. Aanandan, P. Mohanan, and K. Vasudevan, "Wideband printed microstrip antenna for wireless communications," *IEEE Antennas Wireless Propag. Lett.*, vol. 8, pp. 779–781, Jun. 2009.

[11] S. D. Targonski, R. B. Waterhouse, and D. M. Pozar, "Wideband aperture coupled stacked patch antenna using thick substrates," *Electron. Lett.*, vol. 32, no. 21, pp. 1941–1942, Oct. 1996.

[12] S. D. Targonski, R. B. Waterhouse, and D. M. Pozar, "Design of wideband aperture-stacked patch microstrip antennas," *IEEE Trans. Antennas Propag.*, vol. 46, no. 9, pp. 1245–1251, Sep. 1998.

[13] K. Ghorbani and R. B. Waterhouse, "Ultrabroadband printed (UBP) antenna," *IEEE Trans. Antennas Propag.*, vol. 50, no. 12, pp. 1697–1705, Dec. 2002.

[14] H. Oraizi and R. Pazoki, "Radiation bandwidth enhancement of aperture stacked microstrip antennas," *IEEE Trans. Antennas Propag.*, vol. 59, no. 12, pp. 4445–4453, Dec. 2011.

[15] J. M. Kovitz and Y. Rahmat-Samii, "Ensuring robust antenna designs using multiple diverse optimization techniques," in *Proc. IEEE Antennas Propag. Soc. Int. Symp.*, Jul. 2013, pp. 408–409.

[16] Y. S. Chen, W. H. Chou, and S. Y. Chen, "Applications of optimization techniques to designs of ultra-wideband planar monopole antennas," in *Proc. Asia Pacific Microw. Conf.*, Dec. 2012, pp. 714–716.

[17] D. Boeringer and D. Werner, "Particle swarm optimization versus genetic algorithms for phased array synthesis," *IEEE Trans. Antennas Propag.*, vol. 52, no. 3, pp. 771–779, Mar. 2004.

[18] M. A. Panduro and C. A. Brizuela, "A comparative analysis of the performance of GA, PSO and DE for circular antenna arrays," in *Proc. IEEE Antennas Propag. Soc. Int. Symp.*, Jun. 2009, pp. 1–4.

[19] L. Zhang, Z. Cui, Y.-C. Jiao, and F.-S. Zhang, "Broadband patch antenna design using differential evolution algorithm," *Microw. Opt. Technol. Lett.*, vol. 51, no. 7, pp. 1692–1695, 2009.

[20] T. Datta and I. S. Misra, "A comparative study of optimization techniques in adaptive antenna array processing: The bacteria-foraging algorithm and particle-swarm optimization," *IEEE Antennas Propag. Mag.*, vol. 51, no. 6, pp. 69–81, Dec. 2009.

[21] A. Deb, J. S. Roy, and B. Gupta, "Performance comparison of differential evolution, particle swarm optimization and genetic algorithm in the design of circularly polarized microstrip antennas," *IEEE Trans. Antennas Propag.*, vol. 62, no. 8, pp. 3920–3928, Aug. 2014.

[22] H. J. Mohammed *et al.*, "Evaluation of genetic algorithms, particle swarm optimisation, and firefly algorithms in antenna design," in *Proc. 13th Int. Conf. Synthesis Model. Anal. Simul. Methods Appl. Circuit Des.*, Jun. 2016, pp. 1–4.

[23] M. Gregory, S. Martin, and D. Werner, "Improved electromagnetics optimization: The covariance matrix adaptation evolutionary strategy," *IEEE Antennas Propag. Mag.*, vol. 57, no. 3, pp. 48–59, Jun. 2015.

[24] V. Grout, M. O. Akinsolu, B. Liu, P. I. Lazaridis, K. K. Mistry, and Z. D. Zaharis, "Software solutions for antenna design exploration: A comparison of packages, tools, techniques, and algorithms for various design challenges," *IEEE Antennas Propag. Mag.*, vol. 61, no. 3, pp. 48–59, Jun. 2019.
[25] M. Kovaleva, D. Bulger, B. A. Zeb, and K. P. Esselle, "Cross-entropy method for electromagnetic optimization with constraints and mixed variables," *IEEE Trans. Antennas Propag.*, vol. 65, no. 10, pp. 5532–5540, Oct. 2017.
[26] N. Ghassemi, J. Rashed-Mohassel, M. H. Neshati, S. Tavakoli, and M. Ghassemi, "A high gain dual stacked aperture coupled microstrip antenna for wideband applications," *Prog. Electromagn. Res. B*, vol. 9, pp. 127–135, 2008.
[27] C. A. Balanis, *Antenna Theory: Analysis and Design*, 3rd ed. Hoboken, NJ, USA: Wiley, 2005.
[28] J. Jayasinghe, J. Anguera, and D. Uduwawala, "On the behavior of several fitness functions for genetically optimized microstrip antennas," *Int. J. Scientific World*, vol. 3, no. 1, pp. 53–58, 2015.
[29] P. Minvielle, E. Tantar, A. Tantar, and P. Berisset, "Sparse antenna array optimization with the cross-entropy method," *IEEE Trans. Antennas Propag.*, vol. 59, no. 8, pp. 2862–2871, Aug. 2011.
[30] S. Ho and S. Yang, "The cross-entropy method and its application to inverse problems," *IEEE Trans. Magn.*, vol. 46, no. 8, pp. 3401–3404, Aug. 2010.
[31] M. H. Weatherspoon, J. D. Connor, and S. Y. Foo, "Shaped beam synthesis of phased arrays using the cross entropy method," *Int. J. Numer. Model. Electron. Netw. Devices Fields*, vol. 26, no. 6, pp. 630–642, 2013.

**Maria Kovaleva** (Member, IEEE) received the B.S. degree in electrical engineering (Hons) from the Moscow Technical University of Communications and Informatics, Moscow, Russia, in 2011, and the Ph.D. degree in electronics engineering from Macquarie University, Sydney, NSW, Australia, in 2019.

Currently, she is with the Curtin Institute of Radio Astronomy (CIRA), Curtin University, Perth, WA, Australia. Previously, she was a Postdoctoral Research Associate with the Centre for Collaboration in Electromagnetic and Antenna Engineering (C4CELANE) with Macquarie University and an External Lecturer in antennas and propagation with the University of Sydney from 2018 to 2019. From 2011 to 2014, she was an Antenna Design Engineer with the JSC NIIKP (Russian Space Systems), Moscow, Russia. Her current research interests include radio telescopes, aperture arrays, electromagnetic education, evolutionary optimization methods in electromagnetics, and surface electromagnetics.

Dr. Kovaleva was awarded the Macquarie University Vice-Chancellor's Commendation for Academic Excellence for her Ph.D. thesis, TICRA Travel Grant at 2018 IEEE AP-S in Boston, IEEE WIE Travel Grant in 2018, and 2017 Macquarie University Higher Degree Research Award.

**David Bulger** received the B.Sc. (Hons) degree in mathematics from the University of Canterbury, New Zealand, in 1992, the M.Sc.(Dist) degree in mathematics from Massey University, New Zealand, in 1993, and the Ph.D. degree in mathematics from Central Queensland University, Australia, in 1997.

From 1997 to 1999, he worked as a Computer Programmer with Kiwiplan NZ, Manukau, New Zealand, and with Computer Systems Implementation Ltd., Christchurch, New Zealand. He was a Postdoctoral Fellow with Massey University, from 2000 to 2003. Since 2004, he has been with the Statistics Department, Macquarie University, Sydney, Australia. He was Principal Supervisor for three Ph.D. students and a M.Res. student, and Associate Supervisor for two more Ph.D. students. His research interests include statistical applications in public health management, business planning and animal behavior, optimization theory and practice, quantum algorithms, and mathematical and statistical musicology.

Dr. Bulger has won the New Zealand Mathematical Society's annual national Predoctoral Thesis Competition in 1993.

**Karu P. Esselle** (Fellow, IEEE) received the B.Sc. degree in electronic and telecommunication engineering with First Class Honours from the University of Moratuwa, Sri Lanka, and MASc. and Ph.D. degrees with near-perfect GPA in electrical engineering from the University of Ottawa, Ottawa, ON, Canada.

He is currently the Distinguished Professor in electromagnetic and antenna engineering with the University of Technology, Sydney, Australia, and a Visiting Professor with Macquarie University, Sydney, Australia. Previously, he was Director of WiMed Research Centre and Associate Dean–Higher Degree Research (HDR) of the Division of Information and Communication Sciences and directed the Centre for Collaboration in Electromagnetic and Antenna Engineering, Macquarie University. He has authored approximately 600 research publications and his papers have been cited over 9300 times. In each of 2019 and 2018, his publications received over 1100 citations. He has also served as a member of the Dean's Advisory Council and the Division Executive and as the Head of the Department several times. He has provided expert assistance to more than a dozen companies including Intel, Hewlett Packard Laboratory (USA), Cisco Systems (USA), Audacy (USA), Cochlear, Optus, ResMed, and Katherine-Werke (Germany). His team designed the high-gain antenna system for the world's first entirely Ka-band CubeSat made by Audacy, USA and launched to space by SpaceX in December 2018.

Prof. Karu is a Fellow of the Royal Society of New South Wales and Engineers Australia. Since 2018, Karu has been chairing the prestigious Distinguished Lecturer Program Committee of the IEEE Antennas and Propagation (AP) Society. He is also one of the three Distinguished Lecturers (DL) selected by the Society in 2016. He has been serving the IEEE AP Society Administrative Committee in several elected or ex-officio positions since 2015. He is also the Chair of the Board of management of Australian Antenna Measurement Facility, and was the elected Chair of both IEEE New South Wales (NSW) and IEEE NSW AP/MTT Chapter, in 2016 and 2017. He is the first Australian antenna researcher ever to reach Google Scholar h-index of 30 and his citation indices have been among the top Australian antenna researchers for a long time (in March 2020: i10 is 172 and h-index is 47). Karu's awards include 2019 Motohisa Kanda Award (from IEEE USA) for the most cited paper in IEEE TRANSACTIONS ON EMC in the past five years, 2019 Macquarie University Research Excellence Award for Innovative Technologies, 2019 ARC Discovery International Award, 2017 Excellence in Research Award from the Faculty of Science and Engineering, 2017 Engineering Excellence Award for Best Innovation, 2017 Highly Commended Research Excellence Award from Macquarie University, 2017 Certificate of Recognition from IEEE Region 10, 2016 and 2012 Engineering Excellence Awards for Best Published Paper from IESL NSW Chapter, 2011 Outstanding Branch Counsellor Award from IEEE headquarters (USA), 2009 Vice Chancellor's Award for Excellence in Higher Degree Research Supervision, and 2004 Innovation Award for best invention disclosure. Karu is in the College of Expert Reviewers of the European Science Foundation (2019–2022) and he has been invited to serve as an international expert/research grant assessor by several other research funding bodies as well, including the European Research Council and national agencies in Norway, The Netherlands, Canada, Finland, Hong-Kong, Georgia, South Africa, and Chile. In addition to the large number of invited conference speeches he has given, he has been an invited plenary/extended/keynote speaker of several IEEE and other conferences and workshops including EuCAP 2020 Copenhagen, Denmark; URSI'19 Seville, Spain; and 23rd ICECOM 2019, Dubrovnik, Croatia. He is an Associate Editor of IEEE TRANSACTIONS ON ANTENNAS PROPAGATION as well as IEEE ACCESS. He is a Track Chair pf IEEE AP-S 2020 Montreal, Technical Program Committee Co-Chair of ISAP 2015, APMC 2011, and TENCON 2013 and the Publicity Chair of ICEAA/IEEE APWC 2016, IWAT 2014, and APMC 2000.